Effects of electron heating and surface rippling on Rayleigh–Taylor instability in radiation pressure acceleration

View Online   Export Citation   CrossMark

X. Z. Wu,[1,2] (ID) Y. R. Shou,[2,a] (ID) Z. B. Guo,[1,a] (ID) H. G. Lu,[1] J. X. Liu[1] D. Wu,[1] (ID) Z. Gong,[3] (ID) and X. Q. Yan[1,4,a]

AFFILIATIONS

[1] State Key Laboratory of Nuclear Physics and Technology, School of Physics, Peking University, Beijing 100871, China
[2] Center for Relativistic Laser Science, Institute for Basic Science, Gwangju 61005, Republic of Korea
[3] Max-Planck-Institut für Kernphysik, Saupfercheckweg 1, Heidelberg 69117, Germany
[4] Collaborative Innovation Center of Extreme Optics, Shanxi University, Shanxi 030006, China

[a] Authors to whom correspondence should be addressed: shou@ibs.re.kr; zbguo@pku.edu.cn; and x.yan@pku.edu.cn

ABSTRACT

The acceleration of ultrathin targets driven by intense laser pulses induces Rayleigh–Taylor-like instability. Apart from laser and target configurations, we find that electron heating and surface rippling, effects inherent to the interaction process, have an important role in instability evolution and growth. By employing a simple analytical model and two-dimensional particle-in-cell simulations, we show that the onset of electron heating in the early stage of the acceleration suppresses the growth of small-scale modes, but it has little influence on the growth of large-scale modes, which thus become dominant. With the growth of surface ripples, a mechanism that can significantly influence the growth of these large-scale modes is found. The laser field modulation caused by surface rippling generates an oscillatory ponderomotive force, directly modulating transverse electron density at a faster growth rate than that of ions and eventually enhancing instability growth. Our results show that when surface deformation becomes obvious, electron surface oscillation at $2\omega_0$ (where ω_0 is the laser frequency) is excited simultaneously, which can be seen as a signature of this mechanism.

I. INTRODUCTION

Over the past decade, radiation pressure acceleration (RPA) has come to be considered as a promising route to produce compact energetic laser-driven ion sources with a satisfactory energy conversion efficiency.[1–3] Indeed, by utilizing this acceleration regime, proton energies near 100 MeV have been obtained in recent experiments.[4,5] Various applications based on laser-driven ion sources have also been explored, including proton radiography,[6] fast ignition,[7,8] neutron generation,[9] and medical therapy.[10] To meet the requirements of some of these applications, the achievement of higher ion energy and the control of ion beam quality still remain outstanding challenges.

There are several factors that strongly influence the RPA process and have severe adverse effects on the quality of the accelerated ion beams, including the effect of the preplasma induced by the laser prepulse,[5] the finite spot effect,[11] and transverse instability.[12–14] In particular, in the well-known light sail (LS) regime,[2,15,16] where an ultrathin target is driven by an intense circularly polarized (CP) laser pulse, transverse density modulation and surface rippling of the target have been observed in multidimensional particle-in-cell (PIC) simulations,[13,14] as well as in experiments.[17] These phenomena are attributed to Rayleigh–Taylor instability (RTI),[12,18–20] which causes a breakdown of target integrity, leading to premature termination of ion acceleration and broadening of ion energy spectra.

To mitigate the effect of RTI, various efforts have been made to investigate how different laser and target configurations, such as laser intensity and duration, and target density and thickness, influence the development of RTI.[21–24] Furthermore, several

advanced configurations, such as single-cycle[25] or elliptically polarized[26] lasers, and curved[27] or mixed-species[28] targets, have been proposed to suppress the instability. Meanwhile, RTI is ubiquitous in many areas of physics, including astrophysics,[29] geophysics,[30] and nuclear physics.[31] Previous extensive studies in inertial confinement fusion have shown that the growth rate of RTI in an ablatively accelerating plasma can be strongly influenced by effects inherent to the interaction processes, such as ablative flow, electron thermal conduction, and the compressibility of the plasma.[32,33] With regard to the LS acceleration process, there are also many inherent effects that are important during the growth of RTI, including strong electron heating[21,24,34] and deformation of the target front surface.[17,19] However, it remains unclear whether these effects, in turn, play an important role in the evolution of RTI itself.

In this paper, the effects of electron heating and surface rippling on RTI are investigated. We show that electron heating in the early stage of instability suppresses the growth of short-wavelength modes (SWMs), with $\lambda_i < 0.5\lambda$, and makes long-wavelength modes (LWMs), with $\lambda_i \geq 0.5\lambda$, dominant, although RTI favors the generation of small-scale modes. Here, λ is the laser wavelength. We propose an analytical model to demonstrate that high electron temperature can suppress the growth of SWMs, whereas it has little impact on the growth of LWMs. These effects of high electron temperature are further confirmed by two-dimensional PIC simulations. Meanwhile, we find that modulation of the laser electric field by surface rippling can give rise to an oscillatory ponderomotive force, which significantly increases the growth rate and simultaneously excites an electron surface oscillation (ESO) at $2\omega_0$, with ω_0 the laser frequency. The enhancement of RTI growth is related to the extent of surface rippling. These findings enrich the understanding of laser-driven RTI and are conducive to finding ways to suppress instability growth and optimize the ion acceleration mechanism.

II. EFFECTS OF ELECTRON HEATING

Suppressing electron heating is difficult in the acceleration process, even when a CP plane laser at normal incidence to the target surface is used.[24,34,35] It has been demonstrated that the growth of RTI mainly contributes to strong electron heating.[21,35] To investigate the effect of electron heating on the development of RTI and facilitate analytical progress, we analyze the influence of high electron temperature first.

A. Theoretical model

The modeling of RTI growth in a uniformly accelerated plasma target with a sharp interface driven by radiation pressure has been reported in a number of studies.[12,18–20] Here, a similar hydrodynamic approach is taken, and the following assumptions are made to investigate the effect of thermal pressure on the evolution of instability: (i) the laser radiation pressure P_0 remains constant along the interface, and modulation of the radiation pressure caused by target deformation is not considered;[18,19] (ii) the perturbed plasma remains quasi-neutral, i.e., $Z\widetilde{n}_i = \widetilde{n}_e$. For simplicity, we assume an initial planar foil in the x–y plane. We consider the ions to be nonrelativistic and the laser pulse to be totally reflected, which is reasonable during the early acceleration stage. For a small transverse ion density

perturbation $\widetilde{n}_i$ in a warm accelerated target with electron temperature T_e, the resulting perturbed forces acting on ions can be expressed as follows:

$$\frac{\partial \widetilde{v}_{ix}}{\partial t} = -\frac{\widetilde{n}_i}{n_{i0}}g, \tag{1}$$

$$\frac{\partial \widetilde{v}_{iy}}{\partial t} = -g\frac{\partial \widetilde{\eta}}{\partial y} - \frac{ZT_e}{m_i n_{i0}}\frac{\partial \widetilde{n}_i}{\partial y}, \tag{2}$$

where g is the acceleration, m_i is the ion mass, Z is the charge number, n_{i0} is the initial target ion density, and $\widetilde{\eta}(y,t)$ is the surface distortion of the target along the x direction. The surface distortion $\widetilde{\eta}$ depends mainly on the modulation of the longitudinal ion velocity,[18] i.e., $\partial \widetilde{\eta}/\partial t = \widetilde{v}_{ix}$. The first and second terms on the right-hand side of Eq. (2) represent the driving force of RTI and the thermal pressure effect, respectively.

To close the equations, we also need the continuity equation $\partial \widetilde{n}_i/\partial t + n_{i0}\partial \widetilde{v}_{iy}/\partial y = 0$. We take the Fourier transform by assuming that all quantities are $\propto \exp[i(k_y y - \omega t)]$, and, after some further calculations, we obtain the dispersion relation

$$\omega^2 - \frac{k_y^2 g^2}{\omega^2} = k_y^2 c_s^2, \tag{3}$$

where $c_s = \sqrt{ZT_e/m_i}$ is the ion acoustic speed. The root of Eq. (3) is written as $\omega = \omega_r + i\gamma$, where the imaginary part γ can be viewed as the instability growth rate. This dispersion relation has two limiting cases: (i) when $T_e = 0$, $\gamma = \sqrt{gk}$, which is the classic RTI case; (ii) when $g = 0$, $\omega_r = kc_s$, which represents the ion acoustic wave. We can also see that the driving force of RTI is given by

$$F_r = -m_i g\frac{\partial \widetilde{\eta}}{\partial y} = -ik\frac{\widetilde{n}_i}{n_{i0}}\frac{m_i g^2}{\omega^2}.$$

Meanwhile, the thermal pressure on the ions is given by

$$F_T = -ikT_e\frac{\widetilde{n}_i}{n_{i0}}\ (Z=1).$$

Comparing these two forces, we find

$$\sigma = \frac{F_T}{F_r} = \frac{T_e \omega^2}{m_i g^2} \propto -k_y T_e. \tag{4}$$

Here, ω^2 is the negative root of the quadratic equation (3), i.e., $\omega^2 = \frac{1}{2}\left(k_y^2 c_s^2 - \sqrt{k_y^4 c_s^4 + 4k_y^2 g^2}\right)$. Thus, we find that the direction of the force F_T is always opposite to that of the driving force F_r, meaning that thermal pressure has a suppressive effect on the growth of RTI. We solve Eq. (4) numerically and plot the dispersion relation in Fig. 1. When the electron temperature T_e increases, the suppressive effect becomes more obvious for SWMs. When the wavenumber k is small, thermal pressure plays an insignificant role, even if the electron temperature T_e is high. Thus, our model shows that a high electron temperature can suppress the growth of SWMs, while it has almost no influence on the growth of LWMs.
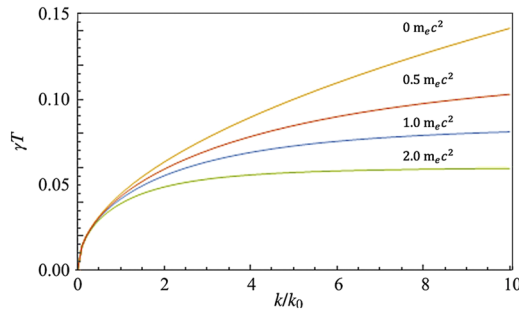
FIG. 1. Dispersion relation for the case $g = 0.002c^2/\lambda$.

B. Simulation results

To verify the above theory, we perform two-dimensional PIC simulations using the SMILEI code.[36] The simulation box is 30λ (x) × 20λ (y), with a resolution of 256 cells/λ, and each cell is filled with 100 particles. A periodic boundary condition is adopted in the y direction. The circularly polarized laser pulse enters the simulation box in the x direction. To reduce electron heating in the interaction process, a uniform transverse profile and flat-top temporal profile with an extremely short rising edge of $1T$ are set for the laser pulse, where T is the laser period. The normalized amplitude of the laser electric field is $a_0 = eE_0/m_e\omega_0 c = 10$, and the pulse duration is $50T$. The target is initialized as a hydrogen foil with thickness $l_0 = 0.2\lambda$ and electron density $n_{e0} = 20n_c$, where n_c is the critical electron density. The areal density of the target is matched with the laser intensity,[15] i.e., $a_0 \sim \pi n_{e0}l_0/n_c\lambda$. Two different initial electron temperatures, namely, $T_{e0} = 0$ and $T_{e0} = 0.2m_ec^2$, are considered to investigate the effect of electron temperature on the instability growth. It should be noted that the thermal pressure in the case of a high electron temperature is still much lower than the radiation pressure in the longitudinal direction.

A comparison of the instability growth for the low-electron-temperature (LET) and high-electron-temperature (HET) cases is shown in Fig. 2. To better understand the growth of different modes, a Fourier analysis of the target areal density is carried out:[37,38]

$$\tilde{n}(k,t) = \left| \int_{-L_y/2}^{L_y/2} \int_0^{L_x} n(x,y,t)e^{iky} \, dx \, dy \right|.$$

Figures 2(a) and 2(b) show the time evolution of the spatial spectra of proton densities for the LET and HET cases, respectively. For the LET case, as the interaction proceeds, the dominant mode k_m, which has the highest amplitude, transforms from an SWM ($k \sim 10k_0$) to an LWM ($k \sim 1k_0$), with $k_0 = 2\pi/\lambda$. This is characteristic of RTI, because SWMs have a higher growth rate than LWMs in the RTI model,[12] namely, $\gamma_{RT} \propto \sqrt{k}$. Similar results have also been observed in many previous simulations.[20,37,38] Since modes with different scales are excited and grow, we can see in Fig. 2(c) a chaotic pattern caused by the superposition of various modes in proton phase space (y, P_y). By contrast, the dominant mode is always around $2k_0$ from the beginning of the linear stage for the HET case. The modulation of the phase space (y, P_y) also shows a regular structure, indicating that SWMs are suppressed in this case.
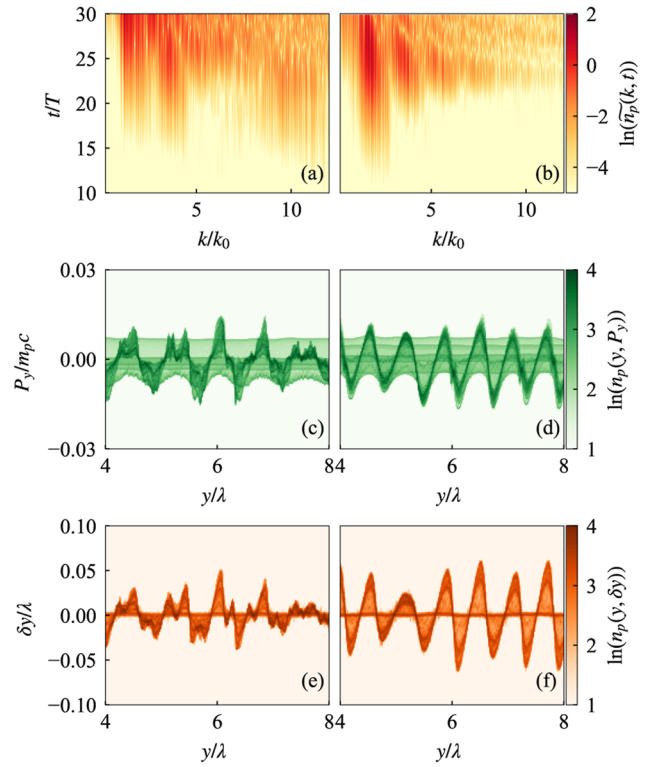

FIG. 2. (a) and (b) Time evolution of spatial proton density $\ln[\tilde{n}_p(k,t)]$ in the transverse direction. (c) and (d) Transverse momentum distribution of protons $\ln[n_p(y, P_y)]$ at $t = 25T$. (e) and (f) Corresponding transverse drift distance of protons $\ln[n_p(y, \delta_y)]$ at $t = 25T$. (a), (c), and (e) are for a cold target; (b), (d), and (f) are for a warm target.

Furthermore, it is found that the maximum proton transverse velocity $v_m \sim 0.01c$ at $t = 25T$ for both cases [Figs. 2(c) and 2(d)]. The ion transverse drift distance, defined as $\delta y = y(t) - y(t_0)$, can be estimated as $\delta y = v_i\tau/2 \sim 0.05\lambda$. Here, $t_0 = 5T$ and $\tau = 20T$. This estimate agrees well with the simulation results shown in Figs. 2(e) and 2(f). Since the ion drift distance is very short ($\delta y \ll 2\pi/k_m = 0.5\lambda$), the fastest ions cannot even traverse small mode wavelengths such as $k = 10k_0$ before $25T$. This is in contrast to previous works in which it was argued that SWMs are suppressed by ion transverse diffusion.[26,38]

Our model not only shows that high electron temperature can suppress the growth of SWMs, but also predicts that it has little influence on the growth of LWMs. To verify this, we plot the time evolution of the amplitudes of different modes $\tilde{n}_p(k,t)$ in Fig. 3. For the LWM $k = 1.9k_0$, $\tilde{n}_p$ grows exponentially, $\tilde{n}_p \propto e^{\gamma t}$, with growth rate $\gamma = 0.49/T$, and the growth rates are almost the same for the LET and HET cases shown in Fig. 3(a). However, for the SWM $k = 3.8k_0$, the growth rate for the LET case is $\gamma = 0.4/T$, but for the HET case, there is almost no initial growth of this mode. It should be noted that the amplitude of this mode grows abruptly at $t = 18T$. This may be because of the strong target modulation induced by the growth of the dominant mode $1.9k_0$. A similar phenomenon was reported when the development of RTI with an initial seed was investigated.[37]
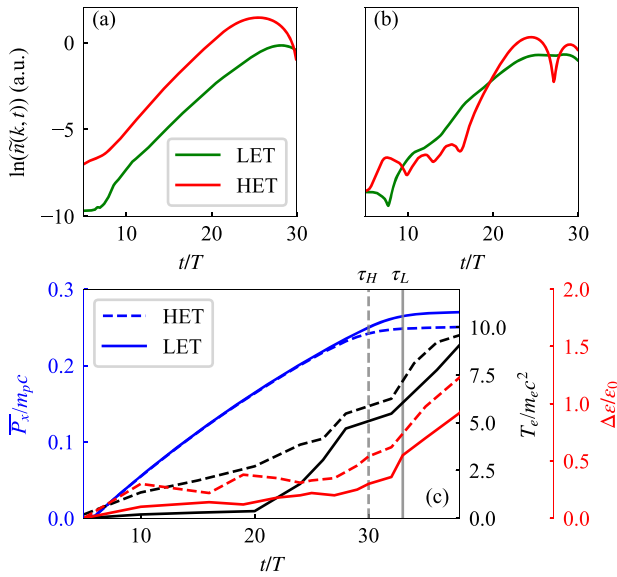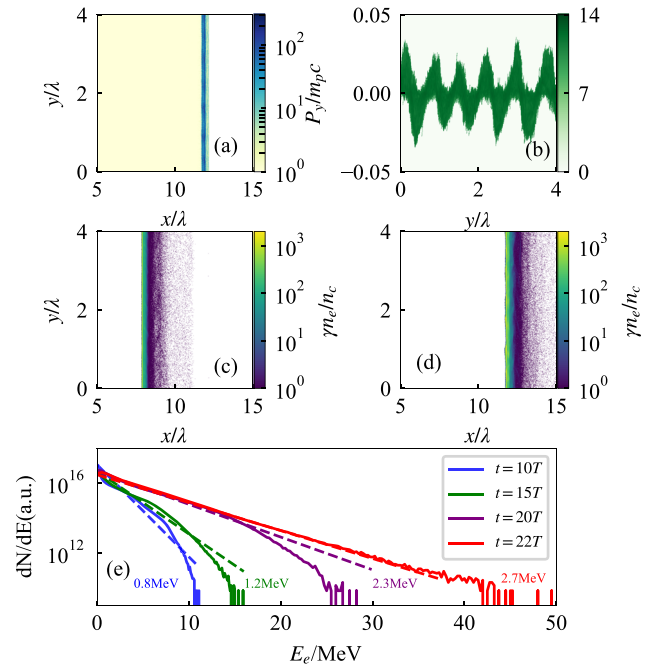
FIG. 3. (a) and (b) Comparison of growth rates at low and high electron temperature for the LWM $k = 1.9k_0$ and the SWM $k = 3.8k_0$, respectively. (c) Temporal evolution of averaged proton longitudinal momentum $\overline{P}_x$ (blue, left axis), electron temperature (black, right black axis), and proton beam energy spread $\Delta\varepsilon/\varepsilon_0$ (red, rightmost axis). Solid and dashed lines represent the LET and HET cases, respectively.

FIG. 4. (a) Proton density profile at $t = 22T$. (b) Proton phase space (y, P_y) distribution at $t = 22T$. (c) and (d) Electron energy distributions at $t = 15$ and $22T$. (e) Time evolution of electron energy spectrum. In this simulation, the target thickness $l_0 = 0.5\lambda$ and the electron density $n_e = 40n_c$. Other simulation parameters are the same as in Fig. 2. The initial electron temperature is set as 10 eV.

A further discussion, however, is outside the scope of this paper.

In the above two simulations, we have focused on the effect of the initial electron temperature T_{e0}. In fact, the electron temperature does not remain the same during the interaction process. In Fig. 3(c), we plot the time evolution of the proton average longitudinal momentum $\overline{P}_x$, the electron temperature T_e, and the energy spread $\Delta\varepsilon_0/\varepsilon$. Radiation pressure continuously accelerates the proton beam with low energy spread until $\tau_H = 30T$ ($\tau_L = 33T$ for the LET case). The electron temperature has begun to increase during the linear stage of instability growth in both the LET and HET cases. This is in agreement with recent work in which it was argued that the development of RTI contributes mainly to the electron heating in the LS ion acceleration process.[21] It should be noted that in our simulations, a plane CP laser with a very short rising edge is employed to suppress the electron heating caused by other mechanisms, such as $\mathbf{J} \times \mathbf{B}$ heating,[39] finite spot effects,[11] and one-dimensional effects.[34] Therefore, we can see that electron heating and the development of RTI influence each other. RTI growth causes stronger electron heating in the acceleration process. Meanwhile, a high electron temperature suppresses only the growth of SWMs, and the growth of LWMs, which are more dangerous for LS acceleration, is hardly affected. Hence, it is found that for the HET case, the LS acceleration is terminated earlier. Even in the LET case, since T_e remains low at the beginning, SWMs are excited and grow, but as the instability develops and the electron temperature increases, some SWMs are prematurely saturated [see Fig. 2(a)].

In Fig. 4, we show that an ultra-thin "cold" target can be heated up to ~MeV in the early stage of instability when an ultra-intense

laser pulse ($a_0 = 60$) is used. The electron temperature T_e reaches 1.2 MeV at $t = 15T$. At this moment, the interaction surface remains flat [see Fig. 4(c)], indicating that it is at the early stage of instability. As instability develops, electron heating increases in strength during the linear stage. Since the early onset of strong electron heating suppresses the growth of SWMs, only the LWM $k_m \sim 0.8k_0$ is excited and grows [see Figs. 4(a) and 4(b)]. This finding is helpful in explaining that although RTI favors the generation of SWMs, the dominant RTI modes observed in many previous simulations are large-scale, especially when the laser intensity is ultra-high.[14,17,19]

III. EFFECTS OF SURFACE RIPPLING

Previous studies have shown that transverse radiation pressure modulation caused by surface rippling can enhance the growth of the mode whose wavelength is close to the laser wavelength, making the laser wavelength a dominant scale.[18,19] Specifically, according to Ref. 19, the modified RTI growth rate for a CP laser is given by

$$\gamma'_{RT} = \gamma_{RT}\sqrt{\frac{K(k)}{2k} + \sqrt{\frac{K(k)^2}{4k^2} + 1}}, \tag{5}$$

where

$$K(k) = \frac{2k_0^2 - k^2}{2\sqrt{k^2 - k_0^2}}.$$

For the mode $k \sim k_0$, $\gamma'_{RT} \gg \gamma_{RT}$, but when $k > \sqrt{2}k_0$, γ'_{RT} turns out to be less than γ_{RT}, indicating that subwavelength mode growth cannot be enhanced by the radiation pressure modulation effect. On the other hand, a dominant scale shorter than the laser wavelength is observed in our simulations ($\sim 0.5\lambda$), as well as in some previous simulations.[19,40] We also notice that the growth rate in the simulations is much higher than the prediction of RTI theory. The growth rate for the dominant mode $k = 1.9k_0$ is $\gamma_s = 0.49/T$, as shown in Fig. 3. However, the corresponding RTI growth rate is $\gamma_{RT} = \sqrt{gk}$ = 0.16/T, and the modified RTI growth rate is only $\gamma'_{RT} = 0.14/T$. The acceleration here is $g = P_0/m_p n_0 l_0 = 0.013c^2/\lambda$, which agrees fairly well with the simulation results. Therefore, the effect of subwavelength surface rippling on instability growth may be related to other more detailed interaction processes.[19]

Owing to the quasi-neutrality assumption adopted in previous RTI models as well as in our model in Sec. II A, the role of electron dynamics in the instability evolution cannot be fully described. It has recently been proposed that the electron–ion coupling effect from density nonuniformity, taking account of the ponderomotive contribution from the term $v_{ey}\partial P_{ey}/\partial y$ in the electron equation of motion, can provide the mechanism for the transverse instability.[24,41] We study the effect of ponderomotive expulsion of electrons induced by surface deformation during the RTI growth. The laser electric field modulation from a deformed interaction surface can give rise to an oscillatory ponderomotive force, which directly modulates the transverse electron motion and significantly enhances the growth of RTI. It is a very complicated task to give a self-consistent theoretical account of the effect arising from the term $v_{ey}\partial P_{ey}/\partial y$ for a growing distorted interface, and so here we give a simple derivation of the ponderomotive force due to surface deformation and discuss how it affects instability growth.

Following the assumptions and derivation in Ref. 19, we consider normal incidence of a CP laser on perfectly reflective

and shallow gratings, which is similar to the situation when RTI grows and the target surface begins to deform. The grating depth η is assumed to be small compared with the laser wavelength. The electric field of the normally incident CP laser is written as $\mathbf{E}_i = (E_{i0}\hat{\mathbf{y}} + iE_{i0}\hat{\mathbf{z}})e^{ik_0x - i\omega_0 t}$. For simplicity, we consider only the field in the y direction. We divide the field into zeroth- and first-order parts: $E_y = E_{y0} + \widetilde{E}_y$. The first-order part $\widetilde{E}_y$ is the modulated electric field caused by surface rippling, which can be represented as[19] $\widetilde{E}_y = -ik\eta E_{i0}e^{iky}$. The zeroth-order electric field $E_{y0} = E_{i0}e^{ik_0x} + E_{r0}e^{-ik_0x}$, which is independent of the position y. Here, E_{i0} and E_{r0} are the zeroth-order electric field intensities for the incident and reflective lasers, respectively. Thus, the ponderomotive force is given by

$$F_p = -v_{ey0}\frac{\partial \widetilde{P}_{ey}}{\partial y} = -\frac{e^2 k^2 \eta}{2\omega_0^2 m_e}E_{y0}E_{i0}e^{iky}(1 - \sin 2\omega_0 t). \quad (6)$$

The enhancement of instability growth comes from the non-oscillatory term of this ponderomotive force, which depends on the extent of rippling, i.e., on $k\eta$. As the rippling grows, the effect of ponderomotive expulsion will become stronger, leading to faster and stronger electron density modulation. The latter enhances transverse ion density fluctuations further, and thus the surface deformation is more severe. A positive feedback loop is formed, and instability growth is enhanced. Meanwhile, the oscillatory term of the ponderomotive force will make some electrons oscillate around the ion density "nodes." Hence, electron surface oscillation (ESO) at $2\omega_0$ can be excited during RT instability growth in the LS acceleration process, although, to the best of our knowledge, this has not been reported so far.

Obviously, the enhancing effect of surface rippling depends on the extent of surface deformation. From Eq. (1) and the equation $\partial\widetilde{\eta}/\partial t = \widetilde{v}_{ix}$, we obtain $\widetilde{\eta} = (g/\omega^2)\widetilde{n}_i/n_{i0}$, which means that both
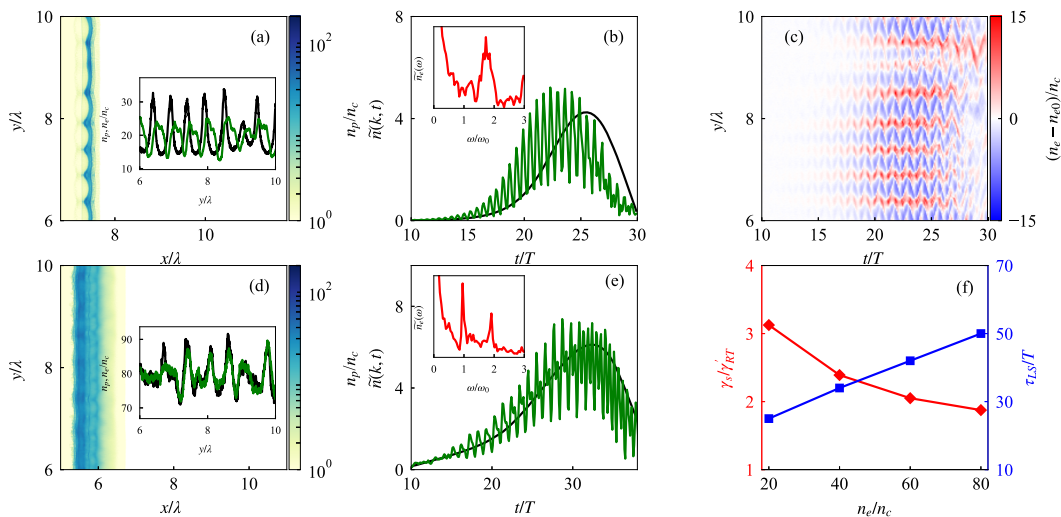

FIG. 5. (a) Proton density profile at $t = 25T$ ($n_{e0} = 20n_c$). The inset shows the transverse electron (green line) and proton (black line) density profiles. (b) Growth of the dominant mode ($k = 1.9k_0$) for electron and protons. The inset shows the Fourier analysis of electron mode growth. (c) Time evolution of transverse electron density fluctuation ($n_e - n_{e0}$). (d) and (e) The same as (a) and (b) but for the case $n_{e0} = 80n_c$. (f) Ratio of the growth rate from simulations and that predicted by RTI theory (red line) and LS termination time (blue line) vs electron density. The dominant mode wavenumbers are $1.9k_0$, $1.4k_0$, $1.1k_0$, and $1.4k_0$, respectively.

the density nonuniformity $\widetilde{n}_i/n_{i0}$ and the acceleration g contribute to surface deformation. When the target density (or thickness) is increased, the acceleration g will decrease and RTI growth will become slower, reducing density modulation. Hence, the surface rippling will become smaller and the enhancement of instability growth will be suppressed.

To confirm the role of surface rippling in laser-driven RTI growth, we perform a series of 2D PIC simulations with targets of different density, while the other parameters remain the same as those in Fig. 2(b). The results are shown in Fig. 5. The enhancement of instability growth is characterized by the excitation and development of $2\omega_0$ transverse ESO. Figure 5(b) shows the growth of the dominant mode ($k = 1.9k_0$) for electron and proton density perturbations for the case $n_{e0} = 20n_c$. The amplitude of electron density perturbation oscillates with a frequency around $2\omega_0$ and grows exponentially at a rate $\gamma_e = 0.55/T$ that is higher than that of protons ($\gamma_p = 0.49/T$). Hence, electrons reach saturation sooner than protons: $t = 23$ vs $25T$. This direct ponderomotive expulsion of electrons enhances RTI growth.

When the electron density is increased to $40n_c$ and to $60n_c$, we still observe a $2\omega_0$ ESO. However, when $n_{e0} = 80n_c$, the acceleration g is decreased further, and only an extremely small surface deformation can be seen in Fig. 5(d). The enhancing effect of the surface rippling on instability growth becomes very limited. The growths of the electron and proton density modulations are almost the same. Since $\widetilde{E}_y$ is very weak, the electron density is modulated transversely by the zeroth-order electric field E_{y0} at the laser frequency [see Fig. 5(e)]. A $2\omega_0$ electron density oscillation is seen after the development of sufficiently large surface deformation in the late stage of instability growth. From Fig. 5(f), we can see that with increasing target electron density, the ratio of the growth rate from the simulation γ_s and the modulated RTI growth rate from RTI theory γ_s' decreases, indicating that the enhancing effect of surface rippling on the growth rate is suppressed, which also agrees well with our prediction. The ratio γ_s/γ_s' can eliminate the influence of the difference between the dominant mode wavenumbers in these cases.

As well as the growth rate, the termination time τ_{LS} of LS acceleration is also employed to show the relationship between the enhancing effect of surface rippling and the electron density in a more straightforward way. In Fig. 6(a), we plot the time evolution of the accelerated proton averaged longitudinal momentum $\overline{P}_x$. According to the equation of motion $dP_x/dt = P_0/m_in_{i0}l_0$, the acceleration g in our simulation agrees with theory for all cases. We define the termination time τ_{LS} as the time at which $\overline{P}_x$ stops growing. As the electron density is increased from $20n_c$ to $80n_c$, the termination time τ_{LS} increases from 25 to $50T$ [see the blue line in Fig. 5(f)]. Furthermore, we see that the termination time is proportional to the electron density, $\tau_{LS} \propto n_{e0}$, suggesting that the instability growth is enhanced by a stronger surface deformation when a lower electron density is used, because the termination time in the traditional RTI theory should be proportional to the square root of the electron density, i.e., $\tau_{LS} \propto \gamma_{RT}^{-1} \propto g^{-1/2} \propto n_{e0}^{1/2}$. For the case $n_e = 80n_c$, the beam quality of a narrow energy spread is maintained for the longest time. However, because the acceleration g is lowest, the longest LS acceleration time cannot yield the highest proton energy. By contrast, for the case $n_e = 20n_c$, since the laser continues to interact with the target after the termination of LS acceleration in our simulation, the
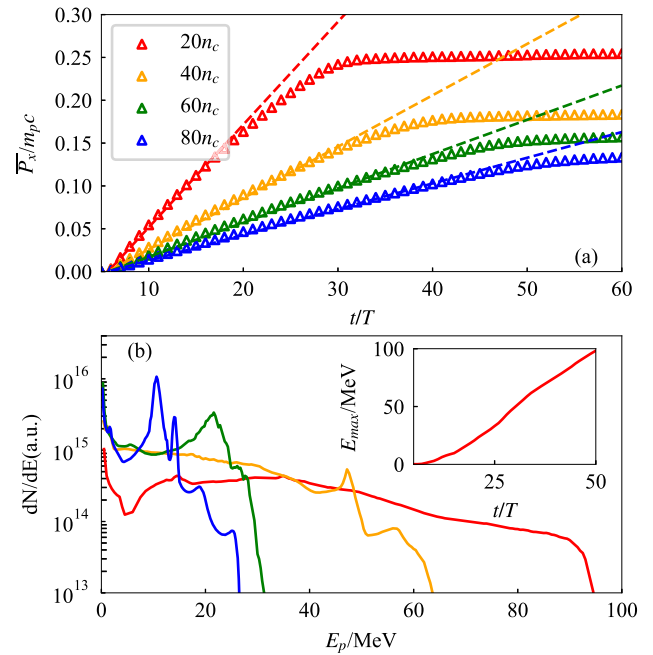
FIG. 6. (a) Temporal evolution of proton average longitudinal momentum $\overline{P}_x$ within the whole simulation box for the cases $n_{e0} = 20n_c$, $40n_c$, $60n_c$, and $80n_c$. The dashed lines show the accelerations in the LS phase, which are $0.012c^2/\lambda$, $0.006c^2/\lambda$, $0.004c^2/\lambda$, and $0.003c^2/\lambda$. (b) Proton energy spectra at $t = 50T$ from 2D simulations with $n_e = 80n_c$ (blue), $60n_c$ (green), $40n_c$ (orange), and $20n_c$ (red). The inset shows the time evolution of the proton cutoff energy for the case $n_e = 20n_c$.

proton cutoff energy is still increasing because of thermal pressure acceleration[42,43] [see the inset in Fig. 6(b)], and thus the highest cutoff proton energy is obtained. Thus, increasing the density could suppress instability growth, but may not be able to increase the proton energy.

In Fig. 7, a large-scale parameter scan is performed to validate the enhancing effects of surface rippling and to show that the LS termination time is related to the electron density. We vary the laser intensity a_0 from 10 to 40. Correspondingly, the areal density $\sigma = n_{e0}l_0$ is changed from σ_{op} to $4\sigma_{op}$ by increasing the density, not the thickness. The optimal areal density $\sigma_{op} = a_0n_c\lambda/\pi$. We find that
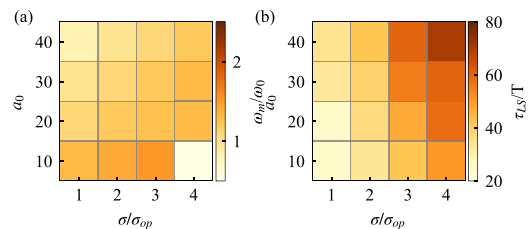
FIG. 7. (a) Dominant frequency of electron density modulation ω_m and (b) LS acceleration termination time τ_{LS} obtained from a series of 2D PIC simulations. The laser intensity a_0 and the areal density $\sigma = n_{e0}l_0$ are varied. For each laser intensity case, the areal density is increased from σ_{op} to $4\sigma_{op}$.

a $2\omega_0$ ESO is excited over a wide range of laser and target parameters. Owing to the Doppler effect, the dominant oscillation frequency ω_m continues to become smaller than $2\omega_0$ as the acceleration g is increased by using a higher laser intensity or a lower target areal density. For each laser intensity, increasing the target density always leads to a longer acceleration time. Counter-intuitively, we also find that in the case of the optimal areal density, as the laser intensity is increased, there is not a reduction in the termination time, which instead becomes a little longer. This suggests that high laser intensity facilitates the stabilization of LS acceleration.[12,22]

Our findings have important implications for optimizing LS acceleration. If the target density is increased, instability is suppressed, but the proton energy cannot be enhanced. Instead of pursuing a longer acceleration time, it could be better to finish ion acceleration with high efficiency and an accelerating gradient within a short time period before the target is destroyed by RTI growth. Our previous work[44] demonstrated that high-power few-cycle lasers possess the advantages of producing higher ion energy with higher laser-to-ion energy conversion efficiency compared with multi-cycle lasers. This is also in agreement with recent work in which it was argued that ultrashort lasers could limit the acceleration time to obtain higher ion energy before the full growth of RTI.[21] With developments in laser technology, particularly the thin-film compression method,[45] high-power few-cycle lasers may be able to fully harness the promise of RPA to produce high-quality ion beams for a wide range of applications.

IV. CONCLUSION

Previous work has shown that the growth of RTI in LS acceleration would cause strong electron heating and surface rippling. In this paper, we have shown that these effects could play an important role in the evolution of RTI itself, indicating that they interact with RTI in a complex way. We have found that electron heating in the early acceleration stage is the main reason why only large-scale instability modes have been observed in numerous LS acceleration simulations. The growth of SWMs is suppressed by high electron temperature, although RTI favors SWM growth. Furthermore, we have found a new mechanism that could significantly enhance the growth of RTI. The laser electric field modulation caused by surface rippling generates an oscillatory ponderomotive force, driving a stronger electron density fluctuation. Fourier analysis has revealed a $2\omega_0$ ESO, which could be seen as a signature of this mechanism. Our results suggest that apart from purely hydrodynamic RTI driven by radiation pressure, these inherent effects related to electron motion need to be considered to better clarify the mechanism of transverse instability occurring in LS acceleration. These findings improve our understanding of RTI growth in the RPA process and have important implications for the optimization of future laser-driven ion acceleration.

ACKNOWLEDGMENTS

AUTHOR DECLARATIONS

Conflict of Interest

The authors have no conflicts to disclose.

Author Contributions

X. Z. Wu: Conceptualization (equal); Data curation (equal); Formal analysis (equal); Software (equal); Visualization (equal); Writing – original draft (equal). **Y. R. Shou**: Formal analysis (equal); Writing – review & editing (equal). **Z. B. Guo**: Formal analysis (equal); Validation (equal). **H. G. Lu**: Software (equal); Validation (equal); Writing – review & editing (equal). **J. X. Liu**: Software (equal); Visualization (equal). **D. Wu**: Methodology (equal); Visualization (equal). **Z. Gong**: Writing – review & editing (equal). **X. Q. Yan**: Supervision (equal); Writing – review & editing (equal).

DATA AVAILABILITY

The data that support the finding of this study are available from the corresponding author upon reasonable request.

REFERENCES

[1] T. Esirkepov, M. Borghesi, S. V. Bulanov, G. Mourou, and T. Tajima, "Highly efficient relativistic-ion generation in the laser-piston regime," Phys. Rev. Lett. **92**, 175003 (2004).

[2] A. Macchi, S. Veghini, and F. Pegoraro, "'Light sail' acceleration reexamined," Phys. Rev. Lett. **103**, 085003 (2009).

[3] H. Daido, M. Nishiuchi, and A. S. Pirozhkov, "Review of laser-driven ion sources and their applications," Rep. Prog. Phys. **75**, 056401 (2012).

[4] A. Higginson, R. J. Gray, M. King, R. J. Dance, S. D. R. Williamson, N. M. H. Butler, R. Wilson, R. Capdessus, C. Armstrong, J. S. Green, S. J. Hawkes, P. Martin, W. Q. Wei, S. R. Mirfayzi, X. H. Yuan, S. Kar, M. Borghesi, R. J. Clarke, D. Neely, and P. McKenna, "Near-100 MeV protons via a laser-driven transparency-enhanced hybrid acceleration scheme," Nat. Commun. **9**, 724 (2018).

[5] I. J. Kim, K. H. Pae, I. W. Choi, C.-L. Lee, H. T. Kim, H. Singhal, J. H. Sung, S. K. Lee, H. W. Lee, P. V. Nickles, T. M. Jeong, C. M. Kim, and C. H. Nam, "Radiation pressure acceleration of protons to 93 MeV with circularly polarized petawatt laser pulses," Phys. Plasmas **23**, 070701 (2016).

[6] M. Borghesi, D. H. Campbell, A. Schiavi, M. G. Haines, O. Willi, A. J. MacKinnon, P. Patel, L. A. Gizzi, M. Galimberti, R. J. Clarke et al., "Electric field detection in laser-plasma interaction experiments via the proton imaging technique," Phys. Plasmas **9**, 2214–2220 (2002).

[7] M. Roth, T. E. Cowan, M. H. Key, S. P. Hatchett, C. Brown, W. Fountain, J. Johnson, D. M. Pennington, R. A. Snavely, S. C. Wilks et al., "Fast ignition by intense laser-accelerated proton beams," Phys. Rev. Lett. **86**, 436 (2001).

[8] M. Okamura, "Laser ion source for heavy ion inertial fusion," Matter Radiat. Extremes **3**, 61–66 (2018).

[9] B. Martinez, S. N. Chen, S. Bolaños, N. Blanchot, G. Boutoux, W. Cayzac, C. Courtois, X. Davoine, A. Duval, V. Horny et al., "Numerical investigation of spallation neutrons generated from petawatt-scale laser-driven proton beams," Matter Radiat. Extremes **7**, 024401 (2022).

[10] S. V. Bulanov, T. Z. Esirkepov, V. S. Khoroshkov, A. V. Kuznetsov, and F. Pegoraro, "Oncological hadrontherapy with laser ion accelerators," Phys. Lett. A **299**, 240–247 (2002).

[11] F. Dollar, C. Zulick, A. G. R. Thomas, V. Chvykov, J. Davis, G. Kalinchenko, T. Matsuoka, C. McGuffey, G. M. Petrov, L. Willingale, V. Yanovsky, A. Maksimchuk, and K. Krushelnick, "Finite spot effects on radiation pressure acceleration from intense high-contrast laser interactions with thin targets," Phys. Rev. Lett. **108**, 175005 (2012).

[12] F. Pegoraro and S. V. Bulanov, "Photon bubbles and ion acceleration in a plasma dominated by the radiation pressure of an electromagnetic pulse," Phys. Rev. Lett. **99**, 065002 (2007).

[13] O. Klimo, J. Psikal, J. Limpouch, and V. T. Tikhonchuk, "Monoenergetic ion beams from ultrathin foils irradiated by ultrahigh-contrast circularly polarized laser pulses," Phys. Rev. Spec. Top.–Accel. Beams **11**, 031301 (2008).

[14] A. P. L. Robinson, M. Zepf, S. Kar, R. G. Evans, and C. Bellei, "Radiation pressure acceleration of thin foils with circularly polarized laser pulses," New J. Phys. **10**, 013021 (2008).

[15] X. Q. Yan, C. Lin, Z. M. Sheng, Z. Y. Guo, B. C. Liu, Y. R. Lu, J. X. Fang, and J. E. Chen, "Generating high-current monoenergetic proton beams by a circularly polarized laser pulse in the phase-stable acceleration regime," Phys. Rev. Lett. **100**, 135003 (2008).

[16] X. Zhang, B. Shen, X. Li, Z. Jin, F. Wang, and M. Wen, "Efficient GeV ion generation by ultraintense circularly polarized laser pulse," Phys. Plasmas **14**, 123108 (2007).

[17] C. A. J. Palmer, J. Schreiber, S. R. Nagel, N. P. Dover, C. Bellei, F. N. Beg, S. Bott, R. J. Clarke, A. E. Dangor, S. M. Hassan *et al.*, "Rayleigh-Taylor instability of an ultrathin foil accelerated by the radiation pressure of an intense laser," Phys. Rev. Lett. **108**, 225002 (2012).

[18] B. Eliasson, "Instability of a thin conducting foil accelerated by a finite wavelength intense laser," New J. Phys. **17**, 033026 (2015).

[19] A. Sgattoni, S. Sinigardi, L. Fedeli, F. Pegoraro, and A. Macchi, "Laser-driven Rayleigh-Taylor instability: Plasmonic effects and three-dimensional structures," Phys. Rev. E **91**, 013106 (2015).

[20] V. Khudik, S. A. Yi, C. Siemon, and G. Shvets, "The analytic model of a laser-accelerated plasma target and its stability," Phys. Plasmas **21**, 013110 (2014).

[21] H.-G. J. Chou, A. Grassi, S. H. Glenzer, and F. Fiuza, "Radiation pressure acceleration of high-quality ion beams using ultrashort laser pulses," Phys. Rev. Res. **4**, L022056 (2022).

[22] B. Qiao, M. Zepf, M. Borghesi, and M. Geissler, "Stable GeV ion-beam acceleration from thin foils by circularly polarized laser pulses," Phys. Rev. Lett. **102**, 145002 (2009).

[23] X. Q. Yan, H. C. Wu, Z. M. Sheng, J. E. Chen, and J. Meyer-ter-Vehn, "Self-organizing GeV, nanocoulomb, collimated proton beam from laser foil interaction at 7×10^{21} W/cm², " Phys. Rev. Lett. **103**, 135001 (2009).

[24] Y. Wan, I. A. Andriyash, W. Lu, W. B. Mori, and V. Malka, "Effects of the transverse instability and wavebreaking on the laser-driven thin foil acceleration," Phys. Rev. Lett. **125**, 104801 (2020).

[25] M. L. Zhou, X. Q. Yan, G. Mourou, J. A. Wheeler, J. H. Bin, J. Schreiber, and T. Tajima, "Proton acceleration by single-cycle laser pulses offers a novel monoenergetic and stable operating regime," Phys. Plasmas **23**, 043112 (2016).

[26] D. Wu, C. Y. Zheng, B. Qiao, C. T. Zhou, X. Q. Yan, M. Y. Yu, and X. T. He, "Suppression of transverse ablative Rayleigh-Taylor-like instability in the hole-boring radiation pressure acceleration by using elliptically polarized laser pulses," Phys. Rev. E **90**, 023101 (2014).

[27] M. Chen, A. Pukhov, T. P. Yu, and Z. M. Sheng, "Enhanced collimated GeV monoenergetic ion acceleration from a shaped foil target irradiated by a circularly polarized laser pulse," Phys. Rev. Lett. **103**, 024801 (2009).

[28] T.-P. Yu, A. Pukhov, G. Shvets, and M. Chen, "Stable laser-driven proton beam acceleration from a two-ion-species ultrathin foil," Phys. Rev. Lett. **105**, 065002 (2010).

[29] N. Inogamov, "The role of Rayleigh-Taylor and Richtmyer-Meshkiv instabilities in astrophysics: An introduction," Astrophys. Space Phys. Rev. **10**, 1–335 (1999).

[30] Y. O. El-Dib, G. M. Moatimid, and A. A. Mady, "A novelty to the nonlinear rotating Rayleigh–Taylor instability," Pramana **93**, 82 (2019).

[31] H. Terasaki, T. Sakaiya, K. Shigemori, K. Akimoto, H. Kato, Y. Hironaka, and T. Kondo, "*In situ* observation of the Rayleigh–Taylor instability of liquid Fe and Fe–Si alloys under extreme conditions: Implications for planetary core formation," Matter Radiat. Extremes **6**, 054403 (2021).

[32] M. Tabak, J. Hammer, M. E. Glinsky, W. L. Kruer, S. C. Wilks, J. Woodworth, E. M. Campbell, M. D. Perry, and R. J. Mason, "Ignition and high gain with ultrapowerful lasers," Phys. Plasmas **1**, 1626–1634 (1994).

[33] H. Takabe, K. Mima, L. Montierth, and R. L. Morse, "Self-consistent growth rate of the Rayleigh–Taylor instability in an ablatively accelerating plasma," Phys. Fluids **28**, 3676–3682 (1985).

[34] E. Siminos, M. Grech, S. Skupin, T. Schlegel, and V. T. Tikhonchuk, "Effect of electron heating on self-induced transparency in relativistic-intensity laser-plasma interactions," Phys. Rev. E **86**, 056404 (2012).

[35] B. S. Paradkar and S. Krishnagopal, "Electron heating in radiation-pressure-driven proton acceleration with a circularly polarized laser," Phys. Rev. E **93**, 023203 (2016).

[36] J. Derouillat, A. Beck, F. Pérez, T. Vinci, M. Chiaramello, A. Grassi, M. Flé, G. Bouchard, I. Plotnikov, N. Aunai *et al.*, "SMILEI: A collaborative, open-source, multi-purpose particle-in-cell code for plasma simulation," Comput. Phys. Commun. **222**, 351–373 (2018).

[37] W. Wang, Y. Yin, T. Yu, H. Xu, D. Zou, and F. Shao, "Numerical investigation of the transverse instability on the radiation-pressure-driven foil," Phys. Rev. E **92**, 063111 (2015).

[38] M. Chen, N. Kumar, A. Pukhov, and T.-P. Yu, "Stabilized radiation pressure dominated ion acceleration from surface modulated thin-foil targets," Phys. Plasmas **18**, 073106 (2011).

[39] W. Kruer, *The Physics of Laser Plasma Interactions* (CRC Press, 2019).

[40] M. Chen, A. Pukhov, Z. M. Sheng, and X. Q. Yan, "Laser mode effects on the ion acceleration during circularly polarized laser pulse interaction with foil targets," Phys. Plasmas **15**, 113103 (2008).

[41] Y. Wan, C.-H. Pai, C. J. Zhang, F. Li, Y. P. Wu, J. F. Hua, W. Lu, Y. Q. Gu, L. O. Silva, C. Joshi, and W. B. Mori, "Physical mechanism of the transverse instability in radiation pressure ion acceleration," Phys. Rev. Lett. **117**, 234801 (2016).

[42] B. Shen and Z. Xu, "Transparency of an overdense plasma layer," Phys. Rev. E **64**, 056406 (2001).

[43] B. Qiao, X. F. Shen, H. He, Y. Xie, H. Zhang, C. T. Zhou, S. P. Zhu, and X. T. He, "Revisit on ion acceleration mechanisms in solid targets driven by intense laser pulses," Plasma Phys. Controlled Fusion **61**, 014039 (2018).

[44] X. Z. Wu, Z. Gong, Y. R. Shou, Y. H. Tang, J. Q. Yu, G. Mourou, and X. Q. Yan, "Efficiency enhancement of ion acceleration from thin target irradiated by multi-PW few-cycle laser pulses," Phys. Plasmas **28**, 023102 (2021).

[45] G. Mourou, S. Mironov, E. Khazanov, and A. Sergeev, "Single cycle thin film compressor opening the door to Zeptosecond-Exawatt physics," Eur. Phys. J.: Spec. Top. **223**, 1181–1188 (2014).